Vilnius University

Faculty of Physics

Institute of Photonics and Nanotechnology

Mantas Vaičiulis

INFLUENCE OF HOLE LOCALIZATION ON THEIR TRANSFER IN InGaN QUANTUM STRUCTURES

BACHELOR'S THESIS

Light Engineering

Study programme

Student	Mantas Vaičiulis
Work supervisor	dr Ramūnas Aleksiejūnas
Reviewer	dr Ignas Grigelionis
Institute director	prof Saulius Antanas Juršėnas

Vilnius 2021

Contents

1. Introduction

InGaN is a group III-nitrides semiconductor, which exhibits plethora of useful properties in many fields. InGaN is already established in light emitting diode (LED) sector as a UV and blue light emitter. The ability to alloy GaN with other group III elements allows for tuning the bandgap energy and enables the blue, green and even red LEDs to be manufactured from the same material family. This broad range of tuning could decrease the price of full color screens as well as enable the photovoltaic devices exploiting the entire Sun spectrum, thus increasing their efficiency. But before such devices can be achieved, certain hurdles must be overcome. While InGaN compounds emitting in the violet spectral range are capable of external quantum efficiencies of 90%, this efficiency rapidly decreases as the indium content is increased. This trend is usually referred to as the "green-gap", since we lack efficient light emitting devices around the green spectral range. The cause of this is not entirely known, although several theories have been proposed. Among those possible green gap causes, one is currently actively debated, namely the impact of hole localization to non-radiative carrier recombination. Hole localization in the alloys such as InGaN occurs due to very fundamental reason - random nature of indium atom distribution in the GaN lattice. Therefore, the places with higher indium content are formed locally, leading to lower-than-average bandgap and, thus, the localization sites for electrons and holes.

In this work, we examine the effect of carrier localization on their transport by studying the dependencies of ambipolar diffusion coefficient on photoexcited carrier density in various InGaN structures. We measured the latter dependences as a function of many parameters, including the photoexcitation wavelength (from 380 to 410 nm), temperature (from 12 to 340 K), indium content (from 9 to 21%), and layer thickness (from few nanometers quantum wells to ~50 nm thick layers). To conduct the measurements, a light induced transient grating (LITG) set up was used. This method is unique because it allows for the direct measurement of the diffusion coefficient in semiconductors. This method is non-destructive and does not require any special preparation of the sample as the charge carriers in the sample are generated using a laser beam and all the data is gathered by collecting two parts of a probe beam, which passes the sample. The aim of this work was to measure the listed dependences and to try to interpret them keeping in mind strong disorder effects on carrier transport and recombination.

2. Literature overview

2.1. Non-equilibrium charge carrier dynamics

2.1.1. Charge carrier generation

Non-equilibrium charge carriers in semiconductors can be optically generated by photon absorption when one or several photons are absorbed. This process can be separated into three distinct processes: single photon interband absorption, multiphoton interband absorption, and multiphoton absorption through impurities.

If the incident photon energy $h\nu$ is equal or greater than the bandgap energy of the semiconductor, the photon can be absorbed and its energy transferred to an electron by transferring the electron from the valence band to the conduction band, creating a free electron-hole pair. Also depending on the semiconductor bandgap structure, the generated carrier can experience direct or indirect jump. If the *k*-vector of the minimum of the conduction band and the peak of the valence band is the same – the semiconductor is called a direct bandgap semiconductor and if the *k*-vector is not the same – it is considered an indirect bandgap semiconductor. Generation in direct bandgap semiconductors typically has high absorption coefficients whereas charge carriers in indirect bandgap semiconductors must change their momentum when transferring from the valence to the conduction band. Such interband absorption is only possible with the assistance of lattice vibrations – phonons. Phonon density depends on the lattice temperature. For the photon to be absorbed the photon must meet in space with the phonon, therefore absorption coefficient also depends on temperature.

If the photon energy is lower than that of the bandgap but the light intensity is high enough, it is possible to observe multi-photon absorption. During this process two or more photons are absorbed to excite a single electron. This process heavily depends on light intensity as these multiple photons must meet in time and space to be absorbed together.

Charge carriers can also be generated with the help of impurities or defects. Electrons are generated by ionization of neutral donors and holes by ionization of neutral acceptors. Shallow impurities absorb light in the far-infrared range, while deep impurities – in the infrared range. The absorption coefficient for this mechanism is a few orders of magnitude smaller than the one for the inter-band transition and depends on the density of impurities and the absorption cross-section, which depends on the photon energy.

2.1.2. Charge carrier diffusion

In general, a charge carrier current consists of two components, namely the drift current driven by electric field and diffusion current due to density gradient. Diffusion coefficient D of charge carriers is the material parameter that is used to quantitatively describe the carrier diffusion. Under equilibrium conditions and in a non-degenerate semiconductor, *D* is proportional to carrier mobility μ, as it is expressed by Einstein relation:

$$D = \frac{k_B T}{e}\mu, \tag{1}$$

here k_B is the Boltzmann constant, T – temperature, and e – elementary charge. Charge carrier mobility is defined as a proportionality coefficient between the carrier speed *v* and electric field *E*, $\vec{v} = \mu\vec{E}$. Mobility can also be expressed by the equation:

$$\mu = \frac{e}{m^*}\langle\tau\rangle, \tag{2}$$

here $\langle\tau\rangle$ is an average momentum relaxation time, m^* - the carrier effective mass. Momentum relaxation time depends on dominant carrier scattering mechanism, which depends on sample conditions. For example, carrier scattering by phonons dominate at high temperatures, scattering by other carriers is essential under high carrier densities (e.g. in metals or highly excited semiconductors), while scattering by charged impurities is typical for low temperatures.

Ambipolar diffusion occurs when both electrons and holes are generated in the semiconductor at the same time, for example during the interband absorption. Both electrons and holes diffuse towards the area of lower concentration, however charge carriers (usually electrons) move faster and separate from the other sign charge carriers. This charge separation creates an electric field called Dember field. This electric field binds both sign carriers not allowing for further separation, therefore the diffusivity becomes determined by the slower moving charge carriers. The ambipolar diffusion coefficient D_a is described as

$$D_a = \frac{n+p}{\frac{n}{D_h}+\frac{n}{D_e}}, \tag{3}$$

where n and p are electron and hole concentrations, D_e and D_h are monopolar electron and hole diffusion coefficients, respectively. In a case when $n = p$, we can simplify the ambipolar diffusion coefficient as

$$D_a = \frac{2D_eD_h}{D_e + D_h} \quad (4)$$

Since in most semiconductors $D_e >> D_h$, ambipolar diffusion coefficient can be approximated to $D_a \approx 2D_h$. In cases when carrier densities are considerably unequal $D_a \approx D_e$ if $p >> n$ and $D_a \approx D_h$ if $n >> p$. By knowing the charge carrier lifetime τ_R and diffusion coefficient D, one can define the diffusion length of carriers, i.e. the average distance carriers travel before recombining:

$$L = \sqrt{D\tau_R}. \quad (5)$$

2.1.3. Percolation

The term "percolation" was introduced in 1957 by Broadbent and Hammersley [1] in mathematical problems of the flow of a liquid through a random maze. This effect is not dissimilar in highly doped semiconductor alloys as charge carriers can diffuse through random paths in lower bandgap semiconductor. In general cases when the semiconductor alloy is well ordered, Einstein relation holds, however semiconductors like InGaN are usually grown by randomly constituting a certain percentage of one atom for another. In our case, certain percentage of Ga atoms is replaced by In. If the percentage of constituent atoms is low, the probability of them coming close to each other is low and in order to diffuse charge carriers must overcome potential barriers by either hopping or tunneling. If the part of constituent atoms in the alloy increases, it can lead to these atoms forming quantum channels instead of quantum wells. This greatly increases diffusion as charge carriers no longer need to overcome potential barriers and can instead diffuse along these percolation channels.

2.1.4. Charge carrier recombination

Non-equilibrium charge carriers in semiconductors exist only temporarily. During this period free carriers can diffuse or drift in the presence of electromagnetic field, however eventually recombination still occurs. Non-equilibrium charge carriers in semiconductors recombine by either radiative or non-radiative paths, when the excess energy is released as photons or phonons, respectively. Typically for many semiconductors, the band-to-band recombination is radiative, while recombination via defect states and Auger recombination have non-radiative characteristics.

During bimolecular recombination process electron or hole travels to the other charge carrier in space where the electron then returns from the conduction band to the valence band and the hole returns from the valence band to the conduction band. The shift of the electron from the excited to

the non-excited state produces energy equal to the energy difference between the two states. Since both electron and hole must meet each other in space for the process to initiate, the recombination rate R can be described [2] as

$$\mathrm{R} = B(np - n_i^2), \tag{6}$$

where B is the bimolecular recombination coefficient, which is a material parameter, n and p – non-equilibrium electron and hole densities, n_i – equilibrium charge carrier density. *B* value strongly depends on the material bandgap structure. This process has a much higher probability in direct bandgap semiconductors as it does not require a phonon for the process to take place.

Shockley-Read-Hall recombination is a process where a lattice impurity or a crystal fault traps a charge carrier of one sign, which is then followed by the trapping of a charge carrier of a different sign and the two charger carriers recombine. It can be imagined as an intermediate energy level in the bandgap. If this level is energetically closer to the conduction band, electrons get trapped more quickly than holes, and the recombination rate mainly depends on how long it takes for holes to be captured [3]. This rate can be described as

$$R_{SRH} = \frac{pn - n_i^2}{p + n + 2n_i^2 cosh\left(\frac{E_i - E_F}{k_B T}\right)} N_t \nu_{th} \sigma \tag{7}$$

where E_i and E_F are defect and Fermi energies respectively, N_t – defect density, ν_{th} – thermal drift velocity, σ – charge carrier trapping cross-section.

Auger recombination is a three particle non-radiative process. It is like bimolecular recombination as it requires for a hole and electron to recombine; however, the process does not create a photon, instead the energy is transferred to a third particle. The third particle can be either an electron in the conduction band or a hole in the valence band. This third particle is then moved to higher energy state of the corresponding band. Rate for this process can be described [4] as:

$$R_{Auger} = C_1 n^2 p + C_2 p^2 n \tag{8}$$

where C_1 and C_2 are the Auger recombination coefficients for electron-electron-hole (eeh) and electron-hole-hole (ehh) processes, respectively.

2.1.5. Charge carrier localization

Localization plays a very important role in nitride-based devices. It prohibits the charger carriers from reaching dislocations and defects, which act as non-radiative recombination centers [5]. InGaN based LEDs are capable of 90% external quantum efficiency (EQE) despite threading dislocation

densities exceeding 10^8 cm^{-2} [6]. In comparison to other semiconductors, dislocation densities in nitride-based devices exceed dislocation densities in AlGaInP-based LEDs by at least 4 orders of magnitude [7]. It was proposed that localization may be the process limiting non-radiative recombination by preventing carriers from reaching dislocations [8]. There are two main theories to explain localization in InGaN.

One theory which explains this phenomenon deals with compositional variation. These variations can occur anywhere from the smallest scale of a unit cell to random alloy concentration fluctuations of nm range. Calculations of InGaN energy levels inside a unit cell show that two indium atoms sharing the same nitrogen atom decrease the bandgap by 8meV, whereas three and four atoms that share the same nitrogen atom decrease the bandgap by 18 and 29 meV respectively [9]. Larger fluctuations of average composition in InGaN/GaN alloy result in larger bandgap changes of tens of meV [10].

The other theory deals with well width fluctuations arising from structural variations. Due to different quantum well width electron and hole energies can be shifted with respect to the bulk material. The magnitude of this shift depends on the width of the well. Narrower wells give bigger energy changes. For this reason, width variations along the QWs give different potential energies. Taking everything into account, Graham et al. calculated that the smallest possible variation of one monolayer in a 3.3 nm width quantum well containing 25% In can result in the difference of 58 meV [11], which significantly exceeds room temperature k_BT energy.

It is important to mention band degeneracy, as it plays a big part in localization as well as diffusion. Band degeneracy occurs if a lot of donors are introduced in the material, which leads to the rise of the Fermi level which eventually starts to overlap with the conduction band. The approximation of non-degenerate semiconductors breaks down when the Fermi level gets closer than about $4k_BT$ to the valence or the conduction band.

2.2. Group III-nitrides

Generally, the term group III-nitrides describes a family of semiconductors, composed of nitrogen and at least one group III element including aluminum, gallium and indium. Together these elements form binary compounds AlN, GaN, InN, ternary compounds AlGaN, InGaN, InAlN as well as quaternary InGaAlN. Bandgaps for these semiconductors range from 0.8 eV for InN, 3.4 eV for GaN and 6.1 eV for AlN [12]. This broad range as well as direct bandgap makes these materials popular in optoelectronic industry as light sources as well as photovoltaic elements.

Gallium nitride has a bandgap of 3.4 eV which grants it special properties for optoelectronic devices like LEDs, especially ones operating at UV wavelengths [13]. Being able to operate at room temperature makes GaN transistors ideal for power amplification in the microwave region as well as showing promising characteristics in the THz field [14]. Indium gallium nitride is a ternary alloy material produced by substituting a fraction of gallium atoms with indium atoms during the growth process [15]. By using Vegard's law, we can calculate semiconductor energy bandgap dependence on the proportion of its constituents.

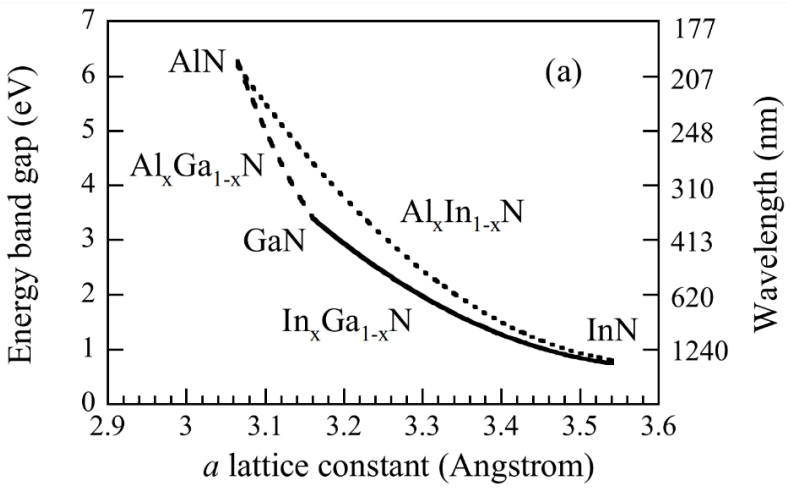

Fig. 1: Vegard's law calculation for AlN, InN and GaN products, their bandgap energy dependence on a lattice constant [16].

Vegard's law is rarely perfectly obeyed as deviations from the linear behavior are usually observed. Despite that, it gives a good starting point for engineering of semiconductor structures. By changing the fraction of indium in the compound it is possible to tune the bandgap from 0.8 to 3.4 eV and in turn tune the wavelength from infrared to ultraviolet. This extreme variability throughout the visible spectrum gives rise to the possibility to create red, green and blue LEDs from a single material. The ability to create full color LEDs from a single material has been sought after property for manufacturing of LED screens. This property is no less desirable in photovoltaic industry as the bandgap is variable throughout the entire sun spectrum and could greatly increase the efficiency of solar cells. $In_xGa_{1-x}N$ with low indium content is already widely used in the industry in production of blue and ultraviolet LEDs as well as semiconductor lasers [17]. It also has been shown that low indium content increases the external quantum efficiency (EQE) of InGaN active layers [18]. In order to achieve single material LEDs, GaN must be doped with higher indium content of 30% or even more in order to decrease the semiconductor bandgap, in turn shifting the emission peak from UV

to green region. The unwanted side effect of increased indium content however, is a drastic drop in EQE, which would be unacceptable in large scale manufacturing of such LEDs.

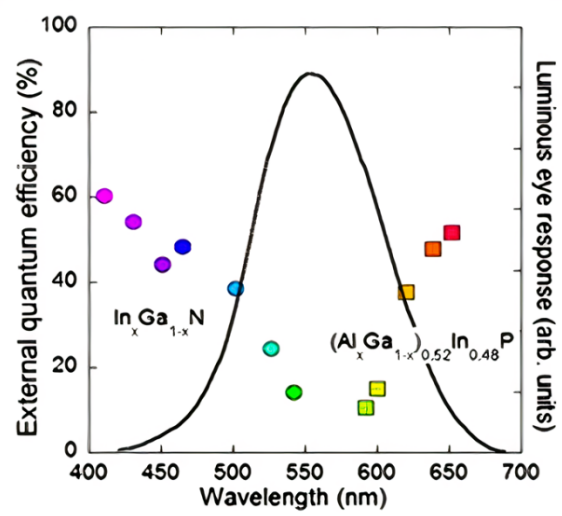

Fig. 2: EQE of LEDs dependance on their wavelength [19].

In Fig. 2 we can see how the external quantum efficiency changes depending on the wavelength. By increasing the indium contents and in turn increasing the emission wavelength we lose EQE as we approach the peak of luminous eye response. Similar effect can be observed in AlGaInP compounds as they too lose EQE by approaching the so called “green-gap” [20]. A proposed reason for this decrease of EQE is hole localization. The basic mechanism for this is the increase of localization energy with the increase of In content in the alloy, which results in the decrease of overlap of electron and hole wave functions [21].

In this work diffusion coefficient was investigated in InGaN samples and its dependance on three separate variables: sample excitation wavelength, sample temperature and In content in the sample. Having measured and fitted the data for layer and quantum well samples we demonstrate LITG measurement results in 4. Results and discussion section.

3. Research methodology

3.1. Samples

In this work, we investigate a number of structures containing InGaN layers of various thicknesses and indium content. A batch of 12 samples was manufactured in University of California, Santa Barbara by James S. Speck's group. All samples were grown by metalorganic chemical vapor deposition (MOCVD) technique on c-plane sapphire substrate. A 3 µm-thick unintentionally doped GaN buffer layer was deposited on QW and layer samples, followed by a 50 nm pure GaN buffer layer. Quantum well samples were grown to have 10 pairs of 3 nm $In_xGa_{1-x}N$ quantum wells. Bulk samples were grown to have a single 45 nm thick $In_xGa_{1-x}N$ layer. Both QW and layer samples then were capped with a protective 12 nm GaN barrier. One sample was produced for reference as a thick 3050 nm GaN layer without any indium. Both QW and layer structure samples contain from 9% to 20% indium.

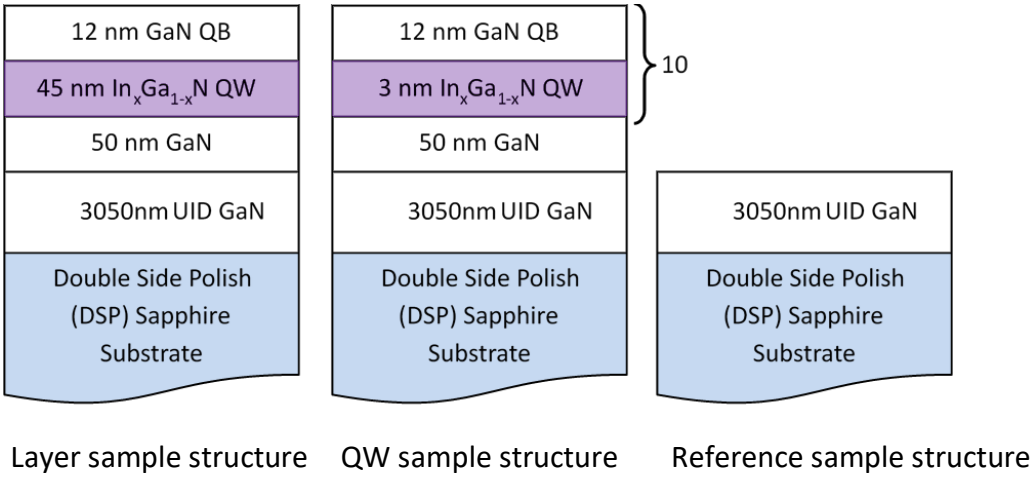

Fig. 3: Structure of measured samples.

3.2. Light induced transient grating

Light induced transient grating (LITG) is a unique method allowing for determination of both carrier lifetime and diffusion coefficient. Granted the ability to directly measure the diffusion length and recombination time in semiconductors, we could calculate the diffusion coefficient [5], however such parameters are impossible to measure simultaneously. At its core, LITG is a pump-probe method. A holographic beam splitter (HBS) is used to split the pump beam into two coherent beams which then excite the sample. The excited area is hit by a probe beam, which can be delayed in relation to the pump beam by a delay line. The probe beam is diffracted from the sample and both

diffracted and transmitted parts of the beam are measured. Simplified LITG measurement setup is shown in Fig. 4.

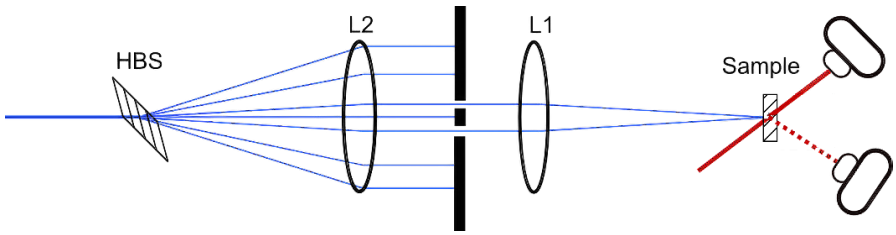

Fig. 4: Simplified view of the measurement setup.

Two coherent pump beams intersect on the sample surface at an angle θ, in turn creating an interference grating pattern with spacing Λ. This modulated excitation pattern generates free carriers, which then create a modulated refractive index as described by the Drude model [22]:

$$\Delta n = -\frac{e^2}{2n_0\omega^2\varepsilon_0}\left(\frac{\Delta N_e}{m_e^*}+\frac{\Delta N_h}{m_h^*}\right), \tag{9}$$

where n_0 is the refractive index of the material, ω is the circular frequency of the incident light, ΔN is excited carrier density, m^* is effective charge carrier mass. This modulated refractive index acts as a diffraction grating for the probe beam Fig. 5.

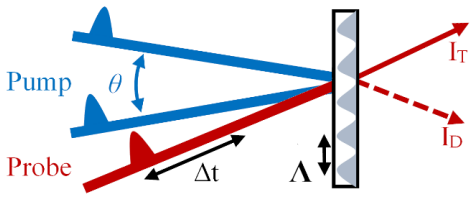

Fig. 5: Absorption of pump beam and both transmission and diffraction of probe beam.

Interference pattern period Λ is calculated as

$$\Lambda = \frac{\lambda}{2\,sin\left(\frac{\Theta}{2}\right)}, \tag{10}$$

where λ – pump beam wavelength, Θ – angle between the two intersecting beams. In this measurement 381 nm wavelength was used for the pump and 1030 nm wavelength for the probe beam. The laser light was generated by a *Pharos* 30 kHz 250 fs laser and amplified using a *ORPHEUS* optical parametric amplifier (OPA). The probe laser beam was taken from the laser, whereas the pump beam was generated through the OPA and a second harmonics crystal. As part of the experiment pump power was attenuated using a pair of gradient filters to achieve pulse energy attenuation from 0.5 to 0.005 μJ. Pump beam dimensions were adjusted using a telescope to make the pump beam diameter at least three times that of the probe beam, so the probe beam would

experience the same excitation conditions on the sample, as it would only pass through the center portion of the gaussian excitation beam. Both diameters were measured using *Thorlabs* CCD camera beam profiler and the data fitted using *Origin* Gaussian function. Two probe beam detectors are required for the measurement – one for the probe beam which passes through the sample and one for the diffracted probe beam. The signal in this experiment is the signal divided by the reference, allowing for noise cancelation resulting in more accurate readings in comparison if only the diffracted beam was measured:

$$\eta = \frac{I_{diffracted}}{I_{transmitted}}. \tag{11}$$

If the probe beam gets delayed by a delay line in relation to the pump beam, we acquire signal kinetics in time (Fig. 6). In certain measurements samples were placed in a vacuum chamber and cooled down to 10 K. This was achieved using a *Cryo Industries* closed-cycle refrigerator system with a *CTI-Cryogenics* helium compressor.

The aim of the experiment is to determine the diffusion coefficient. Since direct measurements are not possible, we instead measure the signal decay in time across several grating periods to determine diffusion rate and recombination time indirectly. Each set of three or four different HBS period measurements taken with the same excitation power would look similar to Fig. 6, where the signal measured with higher period HBS decays slower than the signal measured when using a HBS with a lower period.

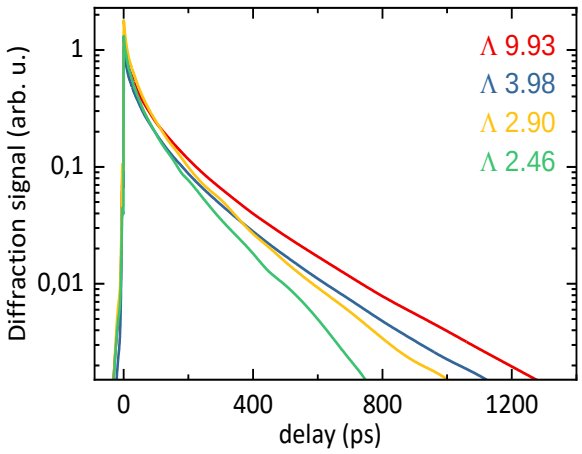

Fig. 6: Measured diffraction signal dependence on probe delay for four different grating mediums.

By plotting the data in logarithmic-linear space, we can determine diffraction grating time τ_G by fitting the diffraction signal in time using a linear fit, as the diffraction signal η decays as an exponential function of τ_G:

$$\eta \propto exp\left(-\frac{2t}{\tau_G}\right). \tag{12}$$

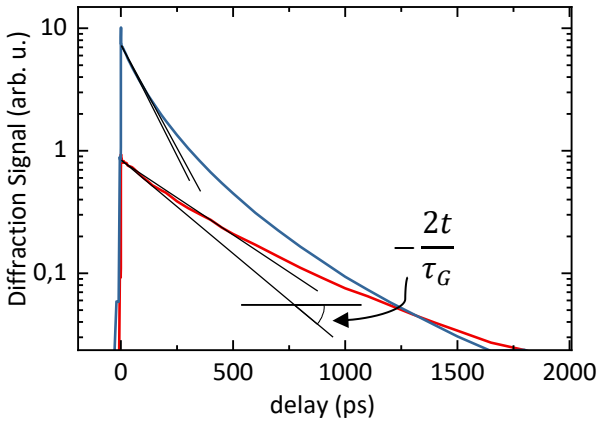

Fig. 7: Visual fit of diffusion signal dependence in time, measured at 500 $\mu J/cm^2$ (blue) and 125 $\mu J/cm^2$ (red) excitation power

In Fig. 7 we can see the usual diffraction signal fitting process. Usually only the least delayed signal can be fitted linearly and for this reason if strongly influenced by the selection of the fitting region. To counteract this effect, each signal is visually fitted at least 3 times and all three results are used in fitting $\frac{1}{\tau_G}$.

At the tail end of the measurement eventually some errors start to appear as the signal strength decreases due to longer delays after excitation resulting in weaker signal, which becomes comparable to background noise (Fig. 9). This decreasing signal raises the need of more datapoints to average, which in turn increases measurement duration. Not all measurements were made to be as smooth as Fig. 6, because most of the time the area which is used to fit τ_G is closer to 1000 ps rather than 6000 ps. Because of this, as a time saving measure longer delayed signal was usually left chaotic as the area of the fit increases to more than 6000 ps only in low excitation powers of below $15\ \mu J/cm^2$ or in samples where diffusion is slower.

Diffraction signal decays due the decay of the diffraction grating in the sample witch is the result of the decaying excited charge carriers. This decay is the result of excited charge carrier recombination and diffusion processes. By fitting diffraction signal dependence on time, we can estimate characteristic diffraction grating time τ_G:

$$\frac{1}{\tau_G} = \frac{1}{\tau_R} + \frac{1}{\tau_D} = \frac{1}{\tau_R} + \frac{4\pi^2 D}{\Lambda^2} \tag{13}$$

here τ_R – recombination time and τ_D – grating decay due to carrier diffusion and Λ – interference pattern period. Equation (13) shows us, that τ_D can be changed by varying the excited carrier grating period. By doing so we can separate the τ_R and τ_D components as we plot $\frac{1}{\tau_G}$ as a function of $\frac{1}{\Lambda^2}$

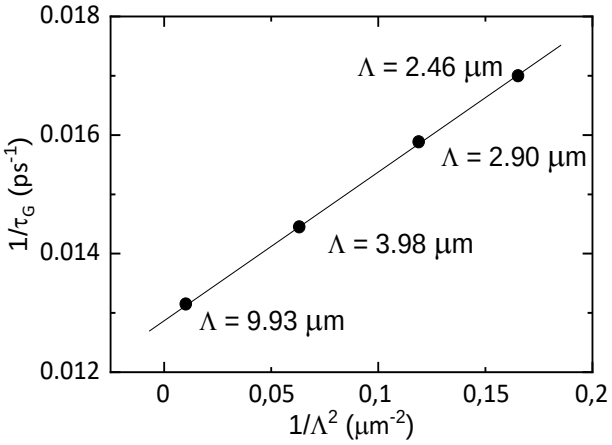

Fig. 8: Dependence of the inverse grating decay time on the inverse of grating period squared.

By fitting inverse τ_G linearly, we acquire both diffusion rate as well as recombination time. In a linear fit τ_R appears as an inverse of the intercept, where D is the slope of the function divided by $4\pi^2$(13). In certain measurement conditions, usually of low temperature and high excitation power, stimulated emission was observer (Fig. 9).

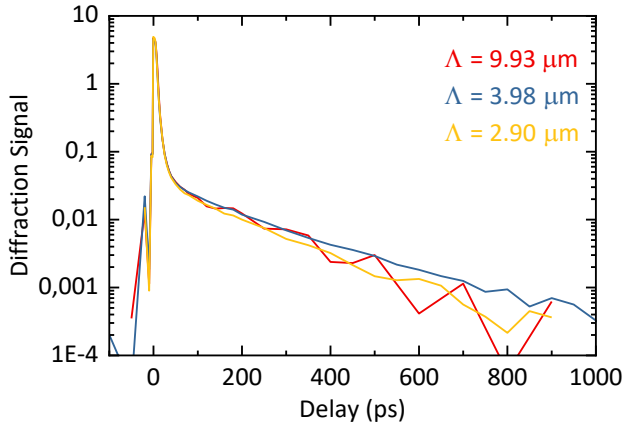

Fig. 9: Observable stimulated emission peak during layer sample measurement at 12K and 577 $\frac{\mu J}{cm^2}$ pump power.

While the process of stimulated emission has its uses in many fields, including laser system creation, it is detrimental to this measurement, because the stimulated emission greatly decreases the free carrier numbers in the sample. This decrease results in data which is unsuited for fitting as it would be inaccurate for the appropriate excitation.

4. Results and discussion

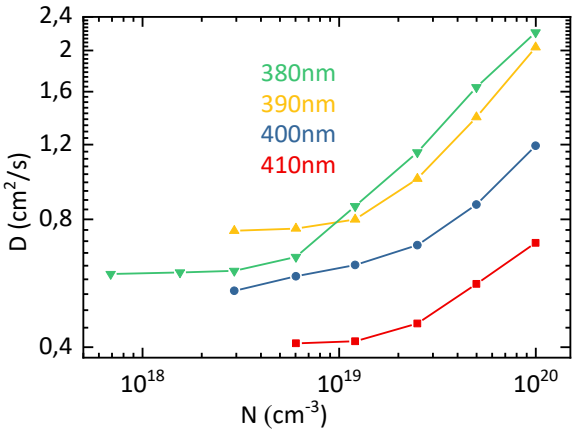

Fig. 10: Dependence of diffusion coefficient on carrier density in $In_{0.1}Ga_{0.9}N$ QW structure of ten 3 nm thick quantum well measured at different excitation wavelengths.

We begin the analysis of diffusion coefficient dependence on photoexcited carrier density *D*(*N*) in QW sample photoexcited with 380 nm light (Fig. 10, green curve). This dependence can be divided into two regions of carrier densities. At low densities, *D*(*N*) remains constant, while around 5×10^{18} cm^{-3} the diffusivity starts to increase with excitation. The first region can be described by simplified Einstein relation (1), valid for nondegenerate semiconductor at equilibrium condition. The increase of *D* with excitation in second region can be attributed to carrier degeneracy, when quasi-Fermi level approaches the bands. T. Malinauskas et. al. invoked the degeneracy to explain the diffusivity increase in GaN [23]. However, it has been shown recently that degeneracy alone is not enough to account for the *D*(*N*) dependence in InGaN; it was assumed that carrier localization to local potential minima formed by random alloy fluctuations was also contributing to this dependence [24]. Carrier delocalization previously was also used to explain *D*(*N*) in InGaN LEDs [25]. For this reason, Ščajev et al. proposed a more complete formula for diffusivity D_{loc} calculations in the presence of degeneracy [26]:

$$D_{loc}(N) = \frac{A(\eta)D_0}{1 + A(\eta)\frac{E_U}{k_B T}\frac{N_L}{N_C}}, \qquad A(\eta) = \frac{F_{1/2}(\eta)}{F_{-1/2}(\eta)}, \qquad \eta = \frac{E - E_F}{k_B T} \tag{14}$$

Here D_0 – low density diffusion coefficient without localization, $F_{\pm 1/2}$ are the Fermi integrals, E_U – Urbach energy, which describes the Gaussian distribution of the localization energy, N_L and N_C –

localized and free carried densities. In the core of this process, one assumes that localized states become occupied and saturated with excitation, thus the ratio between the free and localized carriers grows and *D* also increases (carriers in delocalized states are assumed to be much more mobile).

The impact of carrier localization on diffusion coefficient is also confirmed by measurements of *D*(*N*) at various pump wavelengths with quanta energies just below the bandgap. The lower quanta energy, the deeper localized states are photoexcited. Since carrier mobility is lower in deeper states, *D* should be smaller for longer excitation wavelengths. This exact tendency can be observed in Fig. 10. E.g., low density diffusivity drops from 0.7-0.8 cm^2/s at 380-390 nm to 0.6 cm^2/s at 400 nm and 0.4 cm^2/s at 410 nm. We note that for even longer pump wavelengths no signal was obtained, apparently indicating very low density of deep localized states.

A similar measurement was conducted using QW and layer samples with varying In content. All samples were excited using 380 nm wavelength.

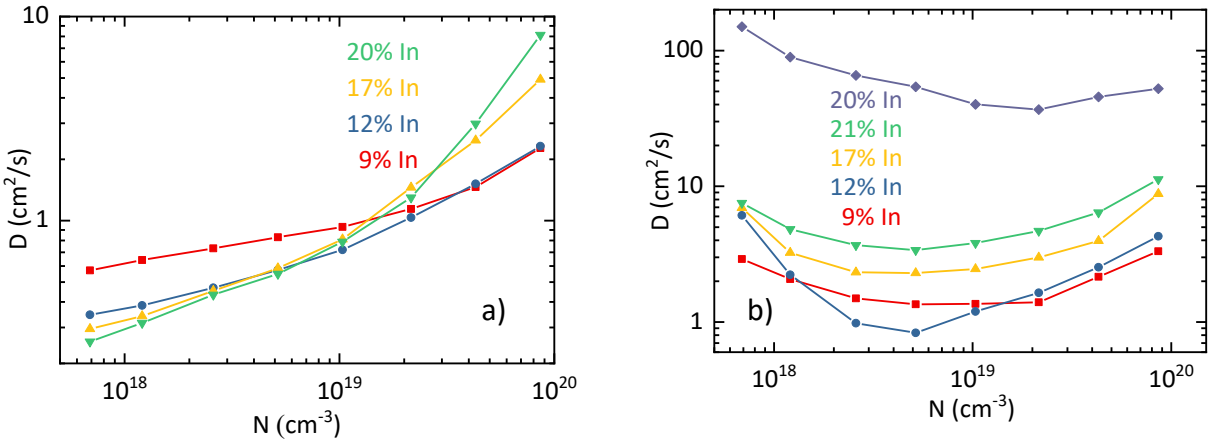

Fig. 11: Diffusion dependence in QWs (a) and layers (b) with different In content on carrier density. QW samples consist of ten 3 nm thick quantum wells, while layer samples are single 50 nm thick layer, except for 21% In sample, which is only 25 nm thick.

QW sample diffusion coefficients respond linearly to increase in excitation power until it approaches a point from which the diffusion coefficient response increases. As mentioned before, the two regions arise from intrinsic degeneracy of the semiconductor and the rise of localization in the presence of high carrier densities. It is noteworthy, that at lowest excitations the samples with lower In content have a higher diffusion coefficient and at highest excitation power this flips and the higher In content sample diffusion coefficients surpass the lower In content samples. This can be attributed to increase of disorder in the semiconductor alloy with the increase of In and consequently the

stronger impact of localization. It has been shown in [26] that *D*(*N*) dependence is steeper in the more disordered material.

9%, 12%, 17% and 21% In layer sample diffusion coefficients vary little from one another over a broad range of carrier densities as well as differ very little from one another. It is notable, that the diffusion coefficient increases with the increase of In content. Diffusion coefficient for 20% In layer sample also varies little over the excitation range, however the diffusion coefficient is nearly an order of magnitude higher than that of any other sample. This exceptionally high value of diffusion coefficient could be explained by the formation of percolation paths through the disorder-induced localized states. Thicker InGaN layer could be the cause of this increased percolation efficiency as the 20% sample is 50 nm thick, while 21% sample is only 25 nm. Simulations show that percolation paths can be the cause of increased current for a given voltage compared to simulations without disorder [27, 28]. All layer samples show three different responses to carrier density. The high diffusion coefficient at low carrier densities could be explained by percolation theory and the decrease of diffusion with the increase of carrier density could be explained by Coulomb blocking in the percolative paths. As the carrier density in these percolative paths increases, so does the Coulomb interaction between the charge carriers which hinders their movement [29, 30]. The center region from 4×10^{18} cm^{-3} to 10^{19} cm^{-3} region in which the slow diffusion coefficient change can be described by Einstein relation (1). The increase of diffusion coefficient at high carrier densities of 10^{19} cm^{-3} and above in layer samples can be attributed to hole diffusion in a degenerate semiconductor with disorder [24].

Finally, *D*(*N*) was measured at various temperatures ranging from 12 to 340 K in the $In_{0.1}G_{0.9}aN$ QW sample at 380 nm pump wavelength, as shown in Fig. 12.

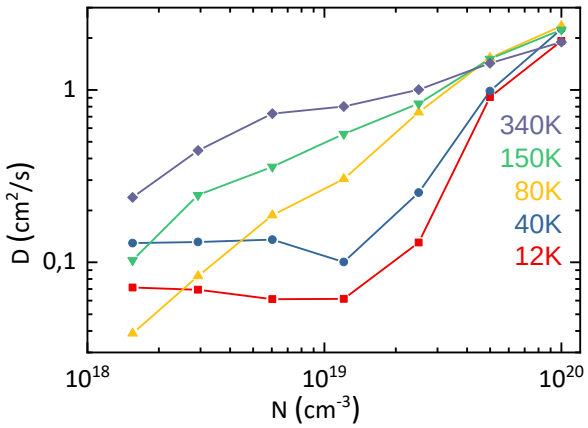

Fig. 12: Diffusion dependence in QW structure of ten 3 nm thick $In_{0.1}Ga_{0.9}N$ quantum wells on carrier density measured at different sample temperatures.

These results disclose the strong dependence of *D(N)* overall shape on temperature. At low temperatures (12 – 40 K), we observe a wide plateau of *D* value up to carrier densities of 10^{19} cm^{-3}, which then is replaced by steep *D* increase at higher densities. In contrast, *D*(*N*) at higher temperatures seems to be more homogeneous, increasing all the time with excitation. These results can also be explained by different contribution of carrier localization to carrier diffusion. In terms of (14), the term E_U/k_BT is large at low temperatures, resulting in low overall *D* values. In general, the diffusion coefficient increases with excitation because the distance between the Fermi level and valence band decreases with carrier density, which allows for easier carrier escape from the localization minima at higher densities. The thermal energy also plays the role in this process, allowing carriers to easier escape those states at higher temperatures. Therefore, the higher carrier densities are needed at lower temperatures to start the efficient thermal release of localized holes, which then is manifested as increase of *D*.

5. Conclusions

1. Ambipolar diffusion coefficient in InGaN structures is a complex function of carrier density, temperature, composition, and layer thickness. Therefore, it cannot be derived from mobility using the simplified Einstein relation.
2. Diffusion coefficient in InGaN structures is strongly affected by structural disorder and consequent hole localization. This is proved by the following experimental facts: decrease of *D* with increasing indium content at low excitations and steeper growth with carrier density at high excitations, smaller *D* values when carriers are photoexcited directly to localized states, and steeper growth of *D* with excitation if compared to that predicted by general Einstein relation002E
3. Diffusion coefficient increases rapidly with increasing InGaN layer thickness, exceeding values of 100 cm^2/s in 50 nm thick $In_{0.2}Ga_{0.8}N$ layer, compared to 10 cm^2/s in 25 nm thick $In_{0.21}Ga_{0.79}N$ layer. This can be explained assuming the efficient carrier diffusion via percolative transport, which becomes more efficient in thicker structures.

6. Santrauka

Mantas Vaičiulis

Skylių lokalizacijos įtaka jų judėjimui InGaN kvantinėse struktūrose

Šio darbo tikslas buvo LITG metodu išmatuoti InGaN kvantinių duobių ir storų sluoksnių struktūras skirtingose sąlygose: naudojant skirtingus žadinančio spindulio bangos ilgius (nuo 380 iki 410 nm), matuojant bandinius su skirtingomis indžio koncentracijomis ir matuojant bandinius skirtingose temperatūrose (nuo 12 iki 340 K) ir iš šių duomenų nustatyti difuzijos koeficiento priklausomybę nuo laisvųjų krūvininkų tankio ir taip nustatyti skylių lokalizacijos įtaka jų judėjimui InGaN kvantinėse struktūrose.

Tyrimui pasirinkti InGaN yra populiari medžiaga puslaidininkinių šviestukų, šviečiančių UV ir mėlynos spalvos regione, gamyboje dėl aukšto išorinio kvantinio našumo, kuris gali siekti iki 90%. Galimybė keisti bangos ilgį ir didelis kvantinis našumas daro šią medžiagą labai patrauklią LED ekranų gamyboje, kadangi teoriškai iš vienos medžiagos galima būtų sukurti tiek mėlynus, tiek žalius ir raudonus šviestukus. Kita labai potenciali sritis yra saulės celių gamyboje, kur keičiamo juostos tarpo puslaidininkiai galėtų būti pritaikyti plačiai saulės spektro daliai. Tačiau, InGaN kenčia dėl stipraus kvantinio našumo kritimo, keičiant bangos ilgį link žalios spalvos. Šis efektas, dar vadinamas žaliuoju tarpu (angl. Green-gap), yra gan gerai aprašytas, tačiau jo priežastys nėra iki galo žinomos. Viena teorija šį efektą aiškina įterptinių indžio atomų sukelta netvarka, kuri savo ruožtu sukelia puslaidininkio išsigimimus, krūvininkų delokalizaciją ir perkoliaciją.

Šiems efektams nagrinėti, buvo tiriami 12 InGaN struktūrų bandinių su indžio koncentracijomis nuo 9 iki 21% juos žadinant nuo 380 iki 400 nm bangos ilgiais prie temperatūrų nuo 12 iki 340 K naudojant LITG metodą. Šis metodas yra unikalus, dėl galimybės tiesiogiai matuoti difuzijos koeficientą puslaidininkiuose. Šis metodas yra ne invazinis ir nereikalauja jokio papildomo bandinių paruošimo, kadangi krūvininkai yra generuojami optiškai ir duomenys yra renkami matuojant zonduojantį spindulį už bandinio.

Ambipolinės difuzijos koeficientas InGaN struktūrose kinta kaip sudėtinga funkcija nuo krūvininkų tankio, temperatūros, puslaidininkio sandaros ir sluoksnio storio. Dėl šios priežasties jo negalima išvesti naudojant supaprastintą Einšteino sąryšį.

Difuzijos koeficientas InGaN struktūrose yra stipriai veikiamas struktūrinės netvarkos ir iš to kylančios skylių lokalizacijos. Ši išvada buvo pasiekta remiantis eksperimentiniais rezultatais: difuzijos koeficiento mažėjimas didinant indžio kiekį esant mažiems krūvininkų tankiams ir statesnio

kilimo esant didelėms krūvininkų koncentracijoms, mažesnės difuzijos koeficiento vertės žadinant tiesiogiai į lokalizuotas būsenas ir statesnis difuzijos koeficiento augimas lyginant su aprašomu standartinėse Einšteino lygtyse.

Pastebėtas greitas difuzijos koeficiento augimas didinant InGaN sluoksnių storį, siekiantis 100 cm^2/s 50 nm storio $In_{0.2}Ga_{0.8}N$ sluoksnyje, lyginant su 10 cm^2/s 25 nm storio $In_{0.21}Ga_{0.79}N$ bandiniu. Šis efektas gali būti paaiškintas perkoliacijos pernašos metodu, kurio efektyvumas auga storesnėse struktūrose.

7. Sources

[1] S. R. Broadbent and J. M. Hammersley, Percolation processes, Mathematical Proceedings of the Cambridge Philosophical Society, 53(03), 629, DOI:10.1017/s0305004100032680

[2] P. T. Landsberg et al., Recombination in semiconductors, Cambridge University Press p.616, 1991

[3] W. Shockley, W. T. Read, Statistics of the Recombinations of Holes and Electrons, Physical Review 87(5) 835–842, 1952, DOI:10.1103/physrev.87.835

[4] P. T. Landsberg, Trap-Auger recombination in silicon of low carrier densities, Appl. Phys. Lett. 50 745, 1987, DOI:10.1063/1.98086

[5] J. Hegarty et al., Studies of exciton localization in quantum-well structures by nonlinear-optical techniques, 1985, J. Opt. Soc. Am. B, DOI:10.1364/josab.2.001143

[6] C. Weisbuch et al., The efficiency challenge of nitride light-emitting diodes for lighting. Physica Status Solidi (A), 1-15, DOI:10.1002/pssa.201431868

[7] S. Nakamura, The Roles of Structural Imperfections in InGaN-Based Blue Light-Emitting Diodes and Laser Diodes, Science, 1998, DOI:10.1126/science.281.5379.956

[8] S. Chichibu et al., Spontaneous emission of localized excitons in InGaN single and multiquantum well structures, Applied Physics Letters 69, 1996, DOI:10.1063/1.116981

[9] S. F. Chichibu et al., Emission mechanisms of bulk GaN and InGaN quantum wells prepared by lateral epitaxial overgrowth, Appl. Phys. Lett., 1999, DOI:10.1063/1.123581

[10] R. Ivanov, Impact of carrier localization on recombination in InGaN quantum wells with nonbasal crystallographic orientations: Doctoral Dissertation, KTH Royal Institute of Technology, 2017, http://www.diva-portal.org/smash/get/diva2:1142091/FULLTEXT02.pdf

[11] D. M. Graham et al., Optical and microstructural studies of InGaNGaN single-quantum well structures, J. Appl. Phys., 2005, DOI:10.1063/1.1897070

[12] R. A. Ferreyra et al., Group III Nitrides, Springer Handbook of Electronic and Photonic Materials, 1–1. DOI:10.1007/978-3-319-48933-9_31

[13] S. N. Mohammad et al., Emerging gallium nitride-based devices, Proceedings of the IEEE, 1995, DOI:10.1109/5.469300

[14] K. Ahi, Review of GaN-based devices for terahertz operation, Optical Engineering, 2017, DOI:10.1117/1.OE.56.9.090901

[15] F. K. Yam and Z. Hassan, InGaN: An overview of the growth kinetics, physical properties and emission mechanisms, Superlattices and Microstructures, 2008, DOI:10.1016/j.spmi.2007.05.001

[16] B. T. Liou et al., Vegard's law deviation in band gaps and bowing parameters of the wurtzite III-nitride ternary alloys, Semiconductor Lasers and Applications II, 2005, DOI:10.1117/12.575300

[17] S. Nakamura et al., High-power InGaN/GaN double-heterostructure violet light emitting diodes, Appl. Phys. Lett., 1993, DOI:10.1063/1.109374

[18] A. G Bhuiyan et al., Indium nitride (InN): A review on growth, characterization, and properties, Journal of Applied Physics, 2003, DOI:10.1063/1.1595135

[19] J. Wu, When group-III nitrides go infrared: New properties and perspectives, Journal of Applied Physics, 2009, DOI:10.1063/1.3155798

[20] W. Shan et al., Band Anticrossing in GaInNAs Alloys, Physical Review Letters, 1999, DOI:10.1103/physrevlett.82.1221

[21] S. Y. Karpov, Carrier localization in InGaN by composition fluctuations: implication to the "green gap", Photonics Research, 5(2), 2017, A7. DOI:10.1364/prj.5.0000a7

[22] J. C. Dainty, Laser-Induced Dynamic Gratings, Springer-Verlag 50, 1986, DOI:10.1007/978-3-540-39662-8

[23] T. Malinauskas et al., Diffusion and recombination of degenerate carrier plasma in GaN, Physica Status Solidi (c), 6(S2), S743–S746, 2009, DOI:10.1002/pssc.200880856

[24] R. Aleksiejūnas et al., Impact of Alloy-Disorder-Induced Localization on Hole Diffusion in Highly Excited c-Plane and m-Plane (In,Ga)N Quantum Wells, Physical Review Applied 14(5):054043, 2020, DOI:10.1103/PhysRevApplied.14.054043

[25] K. Nomeika et al., Impact of carrier localization and diffusion on photoluminescence in highly excited cyan and green InGaN LED structures, Journal of Luminescence, 188, 2017, 301–306, DOI:10.1016/j.jlumin.2017.04.055

[26] P. Ščajev et al., Enhancement in Highly Excited MAPbI3 Perovskite Layers with Additives, The Journal of Physical Chemistry Letters, 9(12), 3167–3172, 2018, DOI:10.1021/acs.jpclett.8b01155

[27] M. Piccardo, Localization landscape theory of disorder in semiconductors. II. Urbach tails of disordered quantum well layers," Physical Review B 95, 2017, DOI:10.1103/PhysRevB.95.144205

[28] T. J. Yang et al., The influence of random indium alloy fluctuations in indium gallium nitride quantum wells on the device behavior, Journal of Applied Physics 116, 2014, DOI:10.1063/1.4896103

[29] H. E. Romero and M. Drndic, Coulomb Blockade and Hopping Conduction in PbSe Quantum Dots, Phys. Rev. Lett. 95, 156801, 2005, DOI:10.1103/PhysRevLett.95.156801

[30] R. E. Chandler et al., Electron transport in quantum dot solids: Monte Carlo simulations of the effects of shell filling, Coulomb repulsions, and site disorder, Phys. Rev. B 75, 085325, 2007, DOI:10.1103/PhysRevB.75.085325